The Effects of Compression and Pore Size Variations on the Liquid Flow Characteristics in Metal Foams

K. Boomsma
ASME Member

D. Poulikakos
ASME Fellow

Laboratory of Thermodynamics in Emerging Technologies,
Institute of Energy Technology,
Swiss Federal Institute of Technology,
ETH Center, 8092 Zurich, Switzerland

Open-cell aluminum foams were investigated using water to determine their hydraulic characteristics. Maximum fluid flow velocities achieved were 1.042 m/s. The permeability and form coefficient varied from $2.46\times10^{-10}\ m^2$ and 8701 m^{-1} to $3529\times10^{-10}\ m^2$ and 120 m^{-1}, respectively. It was determined that the flowrate range influenced these calculated parameters, especially in the transitional regime where the permeability based Reynolds number varied between unity and 26.5. Beyond the transition regime where $Re_K \gtrsim 30$, the permeability and form coefficient monotonically approached values which were reported as being calculated at the maximum flow velocities attained. The results obtained in this study are relevant to engineering applications employing metal foams ranging from convection heat sinks to filters and flow straightening devices. [DOI: 10.1115/1.1429637]

Introduction

This study investigates the hydraulic characteristics of a liquid flowing through a rigid, open-cell, metal foam. The metal foam is an intricately detailed structure, which is manufactured from a variety of molten aluminum processes (Fig. 1(*a*) and Fig. 1(*b*) in uncompressed form and Fig. 1(*c*) and Fig. 1(*d*) in compressed form). The structure of the metal foam opens itself to many applications due to its large surface area to volume ratio and high permeability. The list of possible applications includes lightweight high-strength structural applications, mechanical energy absorbers, filters, pneumatic silencers, containment matrices and burn rate enhancers for solid propellants, flow straighteners, catalytic reactors, heat sinks, and heat exchangers. In addition to flow applications, thermally conductive porous media may also increase the thermal conductance of a solid-fluid system simply by their physical presence [1–3].

The use of open-cell metal foams in fluid-flow applications requires a thorough understanding of the pressure-drop behavior of the fluid flowing through the porous structure. Extensive work has been done to characterize the pressure-drop behavior of fluid flow through porous media, but these are often limited to packed granular beds or beds of packed spheres. An excellent review on the subject involving such granular materials can be found in [4]. As seen in Fig. 1, the structure of the open-cell metal foam is completely different from that encountered in packed beds of spheres. Because of these structural differences, the characterization of the pressure-drop through the open-cell metal foams requires a renewed research effort.

Theory

Different models have been developed in the past 150 years to characterize the fluid flow in a porous matrix on the basis of macroscopically measurable flow quantities. A thorough historical review of the work in porous media can be found in [5]. The first of these models can be traced back to Darcy's publication in 1856 [6]. He established the well-known Darcy's law which states that the pressure-drop per unit length for a flow through a porous medium is proportional to the product of the fluid velocity and the dynamic viscosity (later added by Krüger [7]), and inversely proportional to the permeability.

$$\frac{\Delta p}{L}=\frac{\mu}{K}v \tag{1}$$

However, Darcy's law is applicable only for relatively slow-moving flows, where the permeability-based Reynolds number is small.

$$\mathrm{Re}_K=\frac{\rho\sqrt{K}}{\mu}v<O(1) \tag{2}$$

The velocity term v in Eq. (1) can be either the Darcian velocity of the fluid flow, which is based on the cross-section dimensions of the channel

$$v_D=\frac{Q}{area_{cs}} \tag{3}$$

or the pore (filter) velocity, as given by the Dupuit-Forchheimer relation [8] which accounts for the presence of the solid phase in the channel by dividing the Darcy velocity by the volumetric void fraction of the medium (assuming an isotropic medium).

$$v_p=\frac{v_D}{\varepsilon} \tag{4}$$

Either velocity can be used in the characterization and derivation of the permeability, but one must state which velocity is used in the calculations [4,9,10].

As the flow velocity increases, the form drag becomes more prevalent and must be considered for an accurate description of the pressure-drop [11]. This effect is accounted by the addition of the form drag term C as suggested by Dupuit [12] which yields the following quadratic relation for the pressure-drop.

$$\frac{\Delta p}{L}=\frac{\mu}{K}v+\rho C v^2 \tag{5}$$

This form drag compensation, C, may vary according to the porosity of the medium and the channel which contains it [13]. However, the porous medium container effects of a metal foam do not resemble those generated in packed beds of spheres. In a packed bed of spheres, the porosity of the bed increases exponentially to

Contributed by the Fluids Engineering Division for publication in the JOURNAL OF FLUIDS ENGINEERING. Manuscript received by the Fluids Engineering Division January 29, 2001; revised manuscript received August 24, 2001. Associate Editor: P. W. Bearman.

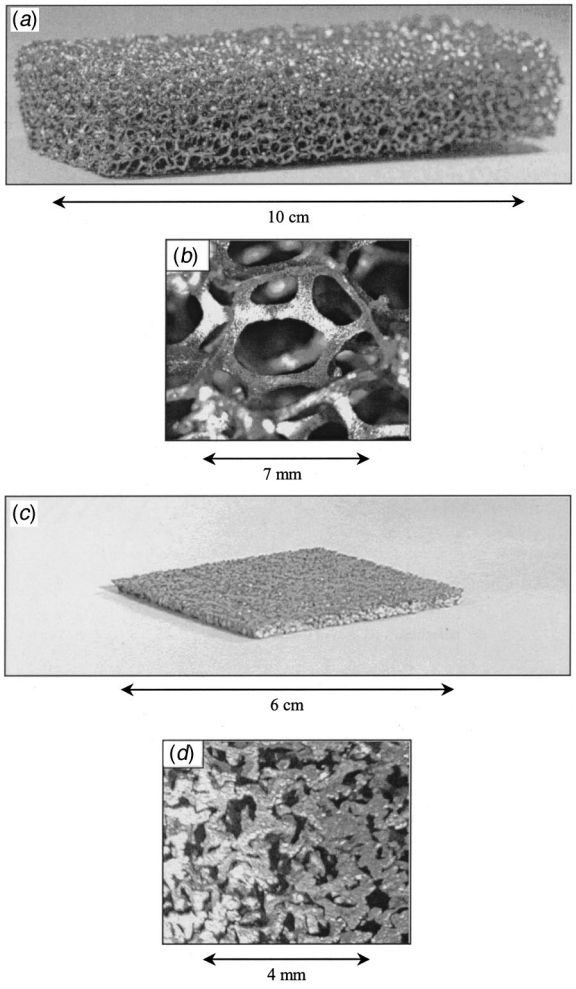

Fig. 1 (*a*) Aluminum foam block which measures 10.0 cm ×4.0 cm×1.5 cm, 92% porous (10 pores per linear inch =6.9 mm pore diameter); (*b*) magnified view of a single pore from Fig. 1 (*a*); (*c*) aluminum foam block as depicted in Fig. 1 (*a*), but compressed by a factor of four, which decreased the porosity from 92% to 76.1%; (*d*) magnified view of the foam in Fig. 1 (*c*).

the container wall [14] causing ''tunneling effects'' which may increase the permeability of the system [15]. This effect, however, is not applicable in the study of the hydraulic characteristics of metal foam because of the metal foam production process. The metal foam production process generates large quantities of liquid foam inside a container whose dimensions are much larger than the pore size. After the foam has been produced in bulk, it is then cut to specification, effectively eliminating any type of wall-interference on the final foam structure. A consistent porosity is thus maintained throughout the foam without the need for any porosity variation considerations [16].

There exists no general relationship between the permeability of a porous medium and porosity because the permeability is affected by the form of the solid structure [4]. Different mathematical models have been developed with varying degrees of success in order to predict the permeability of porous media using simplified structures, with the majority consisting of packed beds of spheres [15,17–19]. However, the structure of the metal foam confronted here is notably more complex than that of a packed bed of spheres. Although some models of flow through various representations of this complex structure have been developed with limited success [20–22], detailed experimentation is still required to accurately measure the permeability of the material.

The addition of the quadratic term in Eq. (5) has been proven to be applicable for packed beds of spheres for permeability based Reynolds number in the range $80>\mathrm{Re}_K>5$ by Dybbs and Edwards [23]. Fand et al. [9] confirmed this for randomly packed spheres, i.e., spheres of various diameters which composed the packed bed instead of spheres of equal diameter which pack regularly. Beyond this Re_K range, Lage et al. [24] demonstrated the existence of a third regime which requires a cubic velocity term for an accurate description of the pressure-drop in metal foams, which is in line with that considered by Forchheimer when studying large sets of hydraulic data from flow through porous media [25].

There are several ways by which the permeability, K, and the form coefficient, C, can be calculated through experimentation. One approach has been to modify Eq. (5) to bring it into linear form and then extrapolate to determine the coefficients as done by Givler and Altobelli [26]. However, this method has been shown to lack accuracy due to the extrapolation, and therefore a more direct and accurate way has been introduced by Antohe et al. [27] using a least-squares quadratic curve fit through the pressure-drop versus fluid-speed data points. A direct advantage of the least-squares curve fit using the form coefficient is the provision for an accurate uncertainty analysis, which is beneficial when analyzing and reporting quantities derived from experimental results. The least squares curve-fitting process works as follows. Making the following substitutions in Eq. (5),

$$A=\frac{\mu}{K} \tag{6}$$

and

$$B=\rho C \tag{7}$$

yields the following quadratic equation for the length-normalized pressure-drop

$$\frac{\Delta p}{L}=Av+Bv^2 \tag{8}$$

in which A and B are solved through the least squares curve fit technique. Applying the least-squares quadratic fit on Eq. (8) gives the following results for the coefficients A and B.

$$A=\frac{\left(\sum_{i=1}^{n}x_iy_i\right)\left(\sum_{i=1}^{n}x_i^4\right)-\left(\sum_{i=1}^{n}x_i^2y_i\right)\left(\sum_{i=1}^{n}x_i^3\right)}{\left(\sum_{i=1}^{n}x_i^2\right)\left(\sum_{i=1}^{n}x_i^4\right)-\left(\sum_{i=1}^{n}x_i^3\right)\left(\sum_{i=1}^{n}x_i^3\right)} \tag{9}$$

$$B=\frac{\left(\sum_{i=1}^{n}x_i^2y_i\right)\left(\sum_{i=1}^{n}x_i^2\right)-\left(\sum_{i=1}^{n}x_iy_i\right)\left(\sum_{i=1}^{n}x_i^3\right)}{\left(\sum_{i=1}^{n}x_i^2\right)\left(\sum_{i=1}^{n}x_i^4\right)-\left(\sum_{i=1}^{n}x_i^3\right)\left(\sum_{i=1}^{n}x_i^3\right)} \tag{10}$$

In these equations, the x_i's represent the various fluid flow velocities at which the data were taken and the y_i's represent the respective measured pressure-drop per unit length values. Knowing A and B, the permeability and inertia coefficient are obtained by backsolving Eq. (6) and Eq. (7).

Experimental Apparatus and Procedure

The experimental setup (Fig. 2) used to measure the pressure-drop for characterization of the metal foams consisted of a foam test housing, a pump to circulate the fluid, various flowrate measuring apparati, two pressure transducers for different pressure ranges, and degassed, deionized water as the working fluid. This setup models that which would use metal foam heat exchangers to cool electronics which dissipate large amounts of heat. The function of the foam test housing was to provide a secure means to

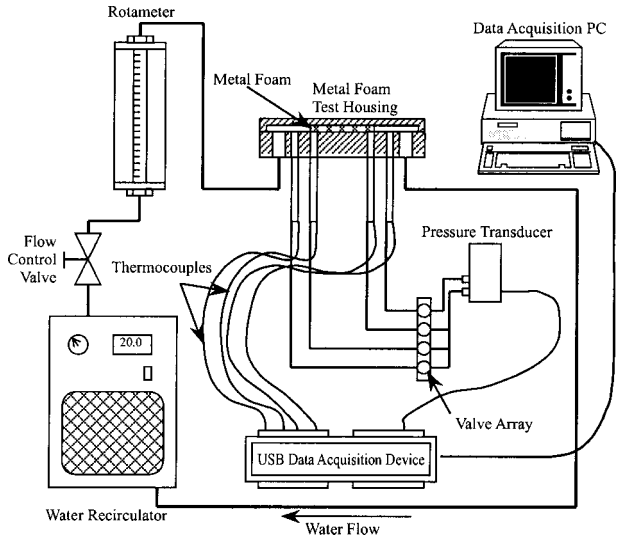

Fig. 2 Diagram of the experimental apparatus used to measure the pressure drop over various configurations of metal foam

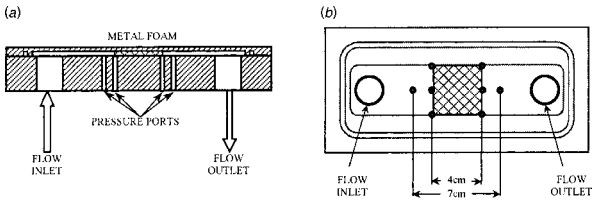

Fig. 3 (*a*) Metal foam test housing cross-sectional view of the inlet, outlet, and foam positioning during the pressure-drop characterization experiments. (*b*) Top view of the metal foam test housing with the lid removed for clarity.

hold the metal foam, to channel the fluid flow through the open-cell metal foam, and to provide a means to measure the pressure-drop across the foam. Figure 3(*a*) is a cross-section of the foam test housing showing the passage of the fluid through the housing and the foam. Figure 3(*b*) shows the same housing but from a top view without the lid for clarity, and allows one to see how the metal foam blocks were placed in relation to the pressure ports located in the bottom of the channel. The foam blocks (measuring 40.0 mm×40.0 mm×2.0 mm) were held securely by means of a tight fit inside the channel. After numerous experiments requiring the changing of the foam blocks by removing the lid, movement of the foam in the channel direction was never observed. The small ports which were drilled into the bottom of the channel were 0.4 mm in diameter and located before and after the foam test pieces, as shown in Fig. 3(*b*). These ports were attached to the pressure transducer through eight different valves which allowed each of the seven pressure ports to be measured directly against the reference port, which was the last port downstream of the water flow. All reported pressures were measured between the two outermost ports, spanning a distance of 7.0 cm. By conservation of mass, the incompressible liquid must accelerate as it enters the foam because the effective cross-sectional area of the channel is reduced by the physical presence of the foam in the channel. The opposite occurs when the liquid leaves the foam; the liquid velocity must decrease in order to compensate the increase in the effective cross-sectional area of the channel. Locating the pressure ports at a distance of 1.5 cm from the entrance and exit of the foam reduced the static pressure-altering effects of the fluid acceleration and deceleration. The six additional ports located at the edge of the foam block were used as a check for symmetry in the pressure. Discrepancies between the left and right hand sides of the pressure measurements during experimentation did not exceed 3%, and were therefore, neglected.

Two different pressure transducers were used depending upon the pressure range of interest. For the lower range, a Huba 692 differential pressure transducer was used for the pressure range between 0.0 and 0.200 bar with an accuracy of ±0.5% FS. For the higher pressure range, an Omega differential pressure transducer (PX81DO-050DT) was implemented for differential pressure measurements up to 3.45 bar with an accuracy of ±0.25% FS. The flowrate was measured with two flowmeters, the Omega FLR 1009 for a flowrate range from 0.0 l/min. to 0.500 l/min, and the Omega FLR 1012 for the flowrate range between 0.500 l/min. and 5.000 l/min. Each flowmeter was calibrated to within ±1.5% FS accuracy. For the larger flowrates attained in the uncompressed foam experiments, a Wisag 2000 rotameter was used for the flowrate range from 1.000 l/min. to 11.220 l/min with ±1% FS accuracy.

The acquisition of the signals from the sensors which included both pressure transducers and two electronic flowmeters was handled by a USB data acquisition device manufactured by IOTech. The device was attached via a USB port on a PC running Windows 98 which controlled the IOTech data acquisition device using LabVIEW software. With this configuration the pressure and flow data were viewed and recorded to the PC hard drive in real time.

A Neslab chiller (CFT-75) pumped water through the foam test housing. It also regulated the water temperature at 20.0°C to within ±0.5°C. The pressure-drop experiments were conducted from the low-end to the high-end of the flowrate range. As a check for hysteresis, selected experiments were performed from the high-end of the flowrate range to the low-end. No hysteresis was observed in these experiments when they were compared to the pressure measurement data taken by varying the flowrate from

Table 1 Compressed foam physical data

Foam	Compression	Name	Expected Porosity [%]	Measured Porosity [%]
5%	2	95-02	90.0	88.2
	4	95-04	80.0	80.5
	6	95-06	70.0	68.9
	8	95-08	60.0	60.8
8%	2	92-02	84.0	87.4
	3	92-03	76.0	82.5
	4	92-04	68.0	76.1
	5	92-05	60.0	72.2
	6	92-06	52.0	66.9

Uncompressed Foam Physical Data

Foam	Pore Diameter [mm]	Specific Surface Area [m^2/m^3]	Measured Porosity [%]
10 PPI	6.9	820	92.1
20 PPI	3.6	1700	92.0
40 PPI	2.3	2700	92.8

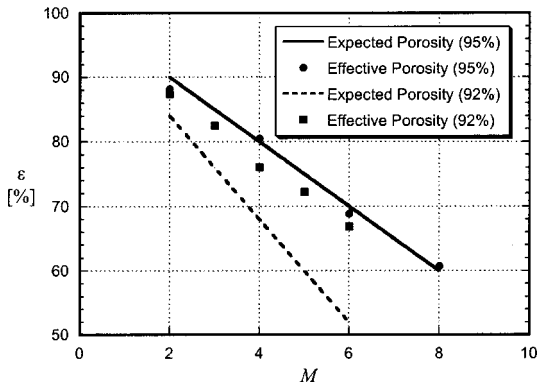

Fig. 4 The expected compressed metal foam porosities based on the precompression porosity and nominal compression factors are graphically compared against the measured values

low to high. Therefore, all data used in the calculations were taken as an average from four experimental trials, adjusting the flowrate from low to high. The temperature of the water during the experiments was held constant at $20.0 \pm 0.5°C$. Within the temperature range of 0.5°C, the physical properties of water do not vary enough to be considered in the calculations when compared to the uncertainties generated by the data acquisition equipment.

Metal Foam. Table 1 gives an overview of the physical properties of all foams which were tested. All foams were manufactured from 6101 aluminum alloy. To generate the array of compressed foam blocks in Table 1, 40 PPI foam (2.3 mm precompression pore diameter) of two different initial porosities, one of 92% and the other of 95%, were compressed by various factors ranging from two to eight. The notation used for the compressed foams works as follows: The first two digits of the foam's name designate the porosity of the foam in pre-compressed form. The second pair of numbers of the foam name after the hyphen signify the compression factor. For example, foam 95-05 designates a foam that was 95% porous in its uncompressed state and then compressed by a factor of six, which in the final compressed state, corresponds to finished foam of one-sixth of its original uncompressed height.

The procedure for compressing the foams, as explained by the manufacturer, allows the foam to expand freely on the open lateral sides of the compression device. By not restraining the lateral edges of the foam block while being compressed, the isotropicity of the aluminum in the foam is claimed to be held more consistent by avoiding mass accumulation along the edges of the compression device. However, as the foam is being compressed, whatever mass of foam extends beyond the original lateral dimensions is lost when the foam is machined to final tolerances, and hence, the measured porosity of the final compressed state of the foam may be higher than expected for a given compression factor because this solid portion of the original foam is lost. To measure the actual values of the porosity, each compressed foam block was weighed, and based on the nominal external measurements, an effective porosity was calculated and compared to an expected final porosity based on the foam's initial solid fraction and compression factor. The expected porosity was based on the simple physical relation for a change in volume, where M is the compression factor (ratio of the original uncompressed foam block height to the final compressed height) and ε is the void fraction of the material $(0 < \varepsilon \leq 1)$.

$$\varepsilon_{\text{compressed}} = 1 - M(1 - \varepsilon_{\text{uncompressed}}) \tag{11}$$

Figure 4 shows the expected porosity of the compressed foam blocks as lines with the actual porosity measurements represented as points. The final overall dimensions of the compressed foam blocks used in the pressure-drop experiments were 40.0 mm × 40.0 mm × 2.0 mm, with the cross-sectional area normal to the flow direction measuring 40.0 mm × 2.0 mm.

In Table 1, the physical characteristics of the three blocks of uncompressed foam are given. The foams are labeled by their characteristic pore diameter in inches (as specified by the manufacturer), which are 10, 20, and 40 pores per linear inch (PPI). However, due to the subjective nature of the pore counting, the uncompressed foams were viewed under a microscope and the pore diameters were measured by hand to an accuracy of ±0.5 mm and tabulated in Table 1. This provides a more objective description of the actual foam geometry for comparison purposes. These foams have open pore diameters of 6.9 mm, 3.6 mm, and 2.3 mm, respectively. Each uncompressed foam block tested was 12.0 mm × 38.0 mm × 80.0 mm, with the flow cross-section measuring 12.0 mm × 38.0 mm. The blocks were cut to final external tolerances by an electro-discharge machining system to minimize deformation of the solid structure and to ensure uniform porosity to the outer edges of each block. The porosity of each block was calculated by dividing its weight by the volume, as measured by the external dimensions, and then comparing this value to the density of the solid metal, aluminum 6101. The surface area to volume ratio (specific surface area) is also tabulated for the uncompressed metal foam blocks in Table 1. This specific surface area data were provided by the foam manufacturer [28].

Results and Discussion

All data were calculated and reported on a Darcian flow velocity basis, as given by Eq. (3). This velocity accounts only for the channel dimensions, is independent of the porosity of the test material, and is practical for comparison against other data sets of porous media. The pressure-drop data for both the compressed and uncompressed foam blocks were taken and normalized on a length-scale basis, which was based on the respective lengths of the foam blocks of 40.0 mm for the compressed metal foams and 80.0 mm for the uncompressed metal foams. From these data, a quadratic curve was fitted through the data points for each foam block according to Eqs. (6)–(10).

Figure 5 shows the pressure-drop experimental data and the fitted curves in graphical form for the compressed blocks based on the Darcian velocity. Figure 5 is separated into (*a*) and (*b*) according to pre-compression porosities of 95% and 92%, respectively. The left-hand ordinate is the length-normalized pressure drop and the right-hand ordinate is the pressure drop for one 40-mm long aluminum foam block. By backsolving the constants A and B from the fitted curves as given in Eqs. (6) and (7), the permeability, form coefficient, and their respective uncertainties, were calculated for each foam block using the entire flowrate range tested for each foam block. This corresponded to a flowrate range of 0.00 l/min. to 5.00 l/min. (0.00 m/s to 1.04 m/s Darcian flow velocity) for the compressed foam. The only exception was foam 95-08. The maximum pressure for the pressure transducer (3.45 bar) was reached with a flow velocity of 0.729 m/s while testing the 95-08 foam block, and therefore, the maximum usable data pair (flow velocity, pressure) in the quadratic least-squares curve fit for foam 95-08 was obtained from this flow velocity value. However, the fitted pressure-drop curve for foam 95-08 was plotted over the entire flow velocity range from 0.00 m/s to 1.04 m/s in Fig. 5(*a*) for comparison purposes. Table 2 gives the permeability, the form coefficient, the A and B coefficients used in the curve fitting procedure, and their respective uncertainties for both the compressed and uncompressed foam blocks.

Reviewing the pressure-drop data from both the compressed and uncompressed foams, it becomes apparent that the flow through open-cell metal foams deviates from Darcy law flow behavior, i.e., the pressure-drop across the foam is a quadratic function of the flow velocity. It is of interest to compare the effects of compression on the permeability and form coefficient for each foam block, which are tabulated in Table 3. As seen in Fig. 5, the

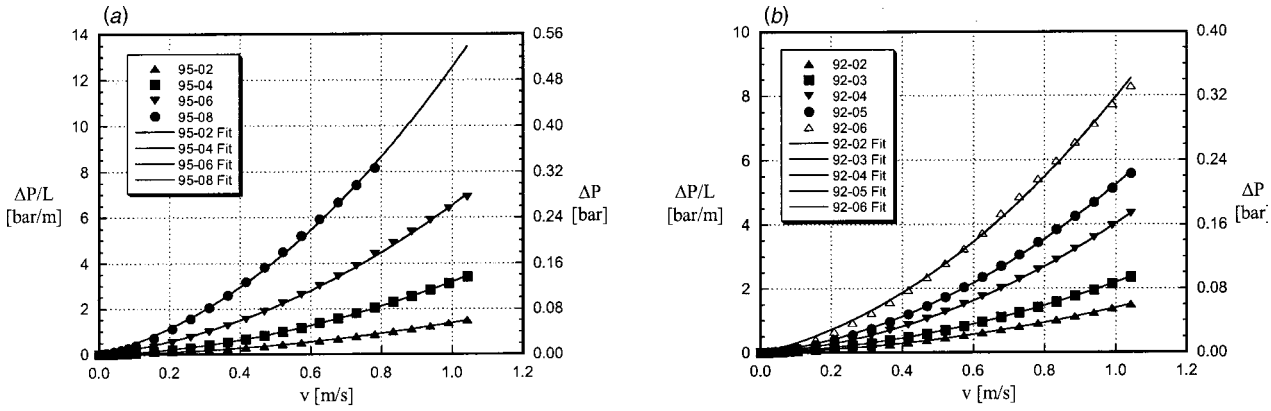

Fig. 5 (*a*) **The experimentally obtained pressure-drop data are plotted along with the fitted curves for the 95-series compressed foam blocks. The experimental uncertainty values are 0.22 bar/m in the length-normalized pressure measurement, 0.0088 bar in the actual pressure measurement, and 0.013 m/s in the fluid flow velocity measurement.** (*b*) **the experimentally obtained pressure-drop data are plotted along with the fitted curves for the 92-series compressed foam blocks. The experimental uncertainty values are 0.22 bar/m in the length-normalized pressure measurement, 0.0088 bar in the actual pressure measurement, and 0.013 m/s in the fluid flow velocity measurement.**

compression has a profound effect on the pressure-drop behavior of a compressed foam. Both foam sample series which were 95% and 92% porous before compression showed similar flow behavior with respect to the changes in the compression factor. For the 95% original porosity series, increasing the compression factor from two to four reduced the permeability from $44.4\times10^{-10}\,m^2$ to $19.7\times10^{-10}\,m^2$, or a relative reduction of 55.6%. Increasing the compression factor from two to six reduced the permeability to a value of $5.25\times10^{-10}\,m^2$, which is a reduction of 88.2%. For the last compressed foam block which was originally 95% porous, increasing the compression factor from two to eight reduced the permeability to $2.46\times10^{-10}\,m^2$, which is a significant reduction of 94.4%.

The other series of compressed foam blocks which where 92% porous before compression showed approximately the same sensitivity between the compression factor and the change in permeability. The first sample, which was compressed by a factor of two, had a measured permeability of $36.7\times10^{-10}\,m^2$. Increasing the compression factor from two to three reduced the permeability to $23.0\times10^{-10}\,m^2$, a reduction of 37.3%. Continuing from a compression factor of two to four, the permeability is reduced to $13.9\times10^{-10}\,m^2$, a reduction of 62.1%. This 62.1% reduction in the compressed foam permeability between a compression factor from two to four is compared with the change in permeability of the 95% porous series between the compression factors of two and four, which is similar at 55.6%. Increasing the compression factor from two to five with the 92% original porosity foam decreased the permeability to $8.07\times10^{-10}\,m^2$, a decrease of 78.0%. The highest compression ratio for the 92% foam series which was tested was six. The permeability at this level of compression was only $3.88\times10^{-10}\,m^2$, which is a reduction of 89.4% when compared to the permeability of the foam of the same initial porosity but with a compression factor of two.

Figure 6 shows a plot of the permeability based on the measured porosity of the compressed metal foam samples. There is no difference made in the plotting of data points between foams of 95% and 92% precompression porosity; all are placed on the same scale by their measured porosity in compressed form. In Fig. 6, the data plot a rather smooth curve. However, the dependence of the permeability on porosity becomes steeper at higher values of porosity. At the low end of the tested porosity range, foam 95-08, with a measured porosity of 60.8%, had a calculated permeability of $2.46\times10^{-10}\,m^2$. Comparing this to the next foam, 92-06, which had a measured porosity of 66.9%, the permeability increased to $3.88\times10^{-10}\,m^2$. An increase in porosity of 6.1% caused an increase in the permeability of 58%. This change in porosity and its associated change in permeability are contrasted to the difference between the two foams which had a compression factor of only two, namely 95-02 and 92-02. The foam 92-02 had a measured porosity of 87.4% and a permeability of $36.7\times10^{-10}\,m^2$. Increasing the porosity by a mere 0.8% to 88.6%, as characterized by foam 95-02, caused the permeability to increase to $44.4\times10^{-10}\,m^2$, an increase of 21%.

The form coefficient also varied with the compression of the

Table 2 Calculated from flow characteristics

Compressed Foam								
Foam	K [10^{-10} m^2]	C [m^{-1}]	A [bar·s/m^2]	B [bar·s^2/m^3]	ΔA [bar·s/m^2]	ΔB [bar·s^2/m^3]	σ_K [%]	σ_C [%]
95-02	44.4	1168	0.216	1.165	0.0291	0.0406	13.5	3.5
95-04	19.7	2707	0.487	2.698	0.0679	0.0946	14.0	3.5
95-06	5.25	4728	1.828	4.714	0.1386	0.1893	7.6	4.0
95-08	2.46	8701	3.893	8.675	0.3269	0.5849	8.4	6.7
92-02	36.7	1142	0.261	1.139	0.0298	0.0412	11.4	3.6
92-03	23.0	1785	0.417	1.780	0.0461	0.0640	11.1	3.6
92-04	13.9	3361	0.689	3.351	0.0856	0.1189	12.4	3.5
92-05	8.07	4073	1.189	4.061	0.1110	0.1529	9.3	3.8
92-06	3.88	5518	2.472	5.502	0.1707	0.2321	6.9	4.2
Uncompressed Foam								
Foam	K [10^{-10} m^2]	C [m^{-1}]	A [bar·s/m^2]	B [bar·s^2/m^3]	ΔA [bar·s/m^2]	ΔB [bar·s^2/m^3]	σ_K [%]	σ_C [%]
10 PPI	3529	120	0.003	0.119	0.0004	0.0098	13.5	8.2
20 PPI	1089	239	0.009	0.239	0.0012	0.0105	13.4	4.4
40 PPI	712	362	0.013	0.361	0.0018	0.0116	13.4	3.2

Table 3 Decrease in permeability [%]

Compression Factor	Foam Series	
M	95	92
2 to 3	--	37.3
2 to 4	55.6	62.1
2 to 5	--	78.0
2 to 6	88.2	89.4
2 to 8	94.4	--

metal foam blocks and the differing pre-compression porosities, ultimately being controlled by the porosity of the compressed metal foam. The form coefficient of the foams increased monotonically with decreasing porosity, with only one exception. Foam 95-02 was the most porous foam tested with a measured porosity of 88.2% and a form coefficient of 1168 m^{-1}. Foam 92-02, which was the second most porous compressed foam tested (87.4%) had a slightly lower form coefficient of 1142 m^{-1}. However, considering the calculated uncertainty of the form coefficients at 3.5%–3.6%, these two values of 1168 m^{-1} and 1142 m^{-1} overlap, thus giving reasonable answers when considering the monotonic increase of the form coefficient with decreasing porosity.

Figure 7 shows the pressure-drop data and associated fitted curves against the Darcian flow velocity for the uncompressed foam blocks. The left-hand ordinate gives the length-normalized pressure-drop, and the right-hand ordinate is the scale of the measured pressure-drop values across the 80 mm-long foam block. The flowrate varied from 1.00 l/min to 11.22 l/min (0.036 m/s to 0.410 m/s Darcian flow velocity) for the uncompressed foam blocks. Table 2 lists the permeability, form coefficient, and their respective uncertainties. The A and B coefficients used in the curve fitting are also listed.

The three aluminum foam blocks which were tested were of nearly the same porosity (within 0.8%). The only difference between the samples was the average pore diameter. Referring to Table 1, the porosities of these uncompressed aluminum foam blocks ranged from 92.0% to 92.8%, and the pore diameter varied from an average of 6.9 mm to 2.3 mm. The difference in pore diameter appeared to dramatically affect the permeability and form coefficient of the foams. Decreasing the pore diameter decreased the permeability and increased the form coefficient. The 10 PPI foam, which had a pore size of 6.9 mm, generated the least flow resistance with a permeability of 3529×10^{-10} m^2 and a form coefficient of 120 m^{-1}. In contrast, the 40 PPI foam with a pore size of 2.3 mm, had the greatest flow resistance with a permeability of 712×10^{-10} m^2 and a form coefficient of 362 m^{-1}. The

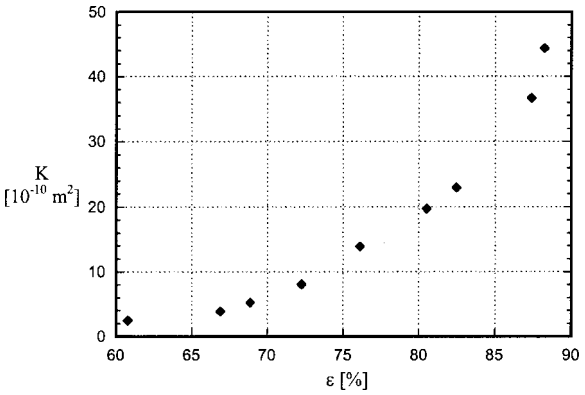

Fig. 6 The permeability of compressed foams is plotted against the values of the measured porosity. The uncertainty values for the permeabilities are gives in Table 2, and the uncertainty value of the measured porosity is estimated at a conservative 3%.

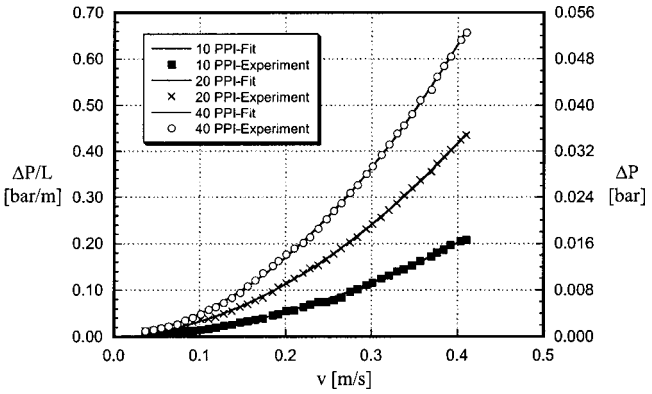

Fig. 7 Pressure-drop versus fluid flow velocity for the three uncompressed metal foams. The experimental uncertainty values are 0.0125 bar/m in the length-normalized pressure measurement, 0.001 bar in the actual pressure measurement, and 0.004 m/s in the fluid flow velocity measurement.

increase in flow resistance directly relates to the "effective surface length" as explained by Lage [5], which relates an increase in drag to the increase in the specific surface area.

Transition From Linear Darcy Regime. An important outcome of this study is the ability to determine when the pressure-drop across a metal foam leaves the linear Darcy regime and enters the form-dominated pressure-drop regime, characterized by the addition of the quadratic term to the linear Darcy law, Eq. (5). Making the substitution of Eqs. (6) and (7) into Eq. (8) and rearranging it into the following form, gives a graphical means by which the linear and nonlinear flow regimes can be separated.

$$\frac{\Delta P}{Lv} = A + Bv \tag{12}$$

The data from the pressure-drop experiments on the uncompressed foam were plotted in Fig. 8 according to Eq. (12) against the fluid flow speed. Figure 8 is separated into parts (a), (b), and (c) depending on the pore diameter as labeled by the foam manufacturer as 10 PPI, 20 PPI, and 40 PPI. In Table 1, these labels correspond to average pore diameters of 6.9 mm, 3.6 mm, and 2.3 mm, respectively. The discrete data points in Fig. 8 are the experimentally obtained data points, and the lines which are shown passing through the points are the second-order curves fitted to the pressure-drop data points using the curve-fitting technique described by Eqs. (5)–(10).

As expected from a quadratic relationship when the coefficients A and B of Eq. (12) are constant, the plotted line has a slope of B and a y-intercept of A. When B is equal to zero, the line is horizontal. This horizontal region describes the pressure-drop region where the form constant, C, is zero and the pressure-drop is governed entirely by Darcy's law, Eq. (1). These two regimes are seen by the discrete experimental points plotted in Fig. 8. In Fig. 8(a–c), the experimental points form a horizontal line in the Darcian flow regime where the flow speeds are less than 0.101 m/s, 0.110 m/s, and 0.074 m/s, respectively. At flow velocities greater than these transitional flow velocity values, the experimental data points turn onto the curve-fitted line with a non-zero slope of B, which by Eq. (7), is the product of the fluid density, ρ, and the form coefficient, C.

The question arises as to which parameter best describes the transition of the pressure-drop from a linear to quadratic curve. A factor commonly used to determine the transition between flow regimes is the Reynolds number, which can be described in three different ways in the area of open-cell metal foams. The first method relates the Reynolds number to the square root of the permeability, K.

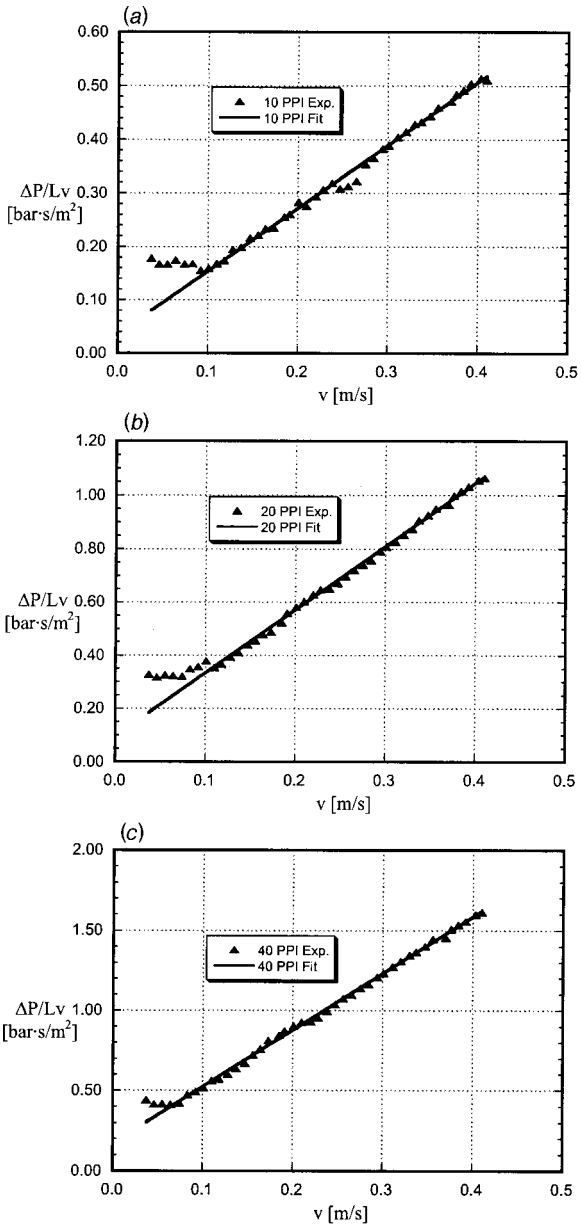

Fig. 8 (*a*) The quantity ($\Delta P/Lv$) for the 10 PPI foam (6.9 mm pore diameter) is plotted to show the pressure-drop deviation from Darcy's law at fluid flow velocities greater than 0.101 m/s. The discrete points represent the experimental data, and the straight line is the corresponding quadratic curve-fit. (*b*) The quantity ($\Delta P/Lv$) for the 20 PPI foam (3.6 mm pore diameter) is plotted to show the pressure-drop deviation from Darcy's law at fluid flow velocities greater than 0.110 m/s. The discrete points represent the experimental data, and the straight line is the corresponding quadratic curve-fit. (*c*) The quantity ($\Delta P/Lv$) for the 40 PPI foam (2.3 mm pore diameter) is plotted to show the pressure-drop deviation from Darcy's law at fluid flow velocities greater than 0.074 m/s. The discrete points represent the experimental data, and the straight line is the corresponding quadratic curve-fit.

$$\mathrm{Re}_K = \frac{\rho v \sqrt{K}}{\mu} \tag{13}$$

However, the value for K may be calculated by two different methods. One method uses the pressure-drop data points from a zero flow velocity value up to and including the velocity at which the transition to the quadratic regime takes place. The second method uses a larger flow velocity range which encompasses the transitional flow velocity by a subjective amount.

The third method bases the Reynolds number on the average pore diameter. In this method, the permeability, K, in Eq. (13) is replaced by the average pore diameter of the respective uncompressed open-cell aluminum foam, as tabulated in Table 1.

$$\mathrm{Re}_p = \frac{\rho v D_p}{\mu} \tag{14}$$

Table 4 Transitional Reynolds number in uncompressed aluminum foams

Foam	D_p [mm]	$v_{transition}$ [m/s]	Re_K (limited)	Re_K (full)	Re_p
10 PPI	6.9	0.101	26.5	62.4	725
20 PPI	3.6	0.110	22.3	37.8	412
40 PPI	2.3	0.074	14.2	20.5	177

Table 4 gives the Reynolds numbers at the transitional flow velocities using these three methods as described above. Using the permeability based on a maximum flow velocity which equals the transitional flow velocity (limited range), the flows for the three open-celled aluminum foams entered the quadratic pressure-drop relationship at Re values of 26.5, 22.3, and 14.2 for the 10 PPI, 20 PPI, and 40 PPI aluminum foams, respectively. These Re values correspond to fluid flow velocities of 0.101 m/s, 0.110 m/s, and 0.074 m/s. These velocities are contrasted to the maximum flow velocity tested, 0.410 m/s. This maximum velocity was used in the second method (full range) and generated a larger spread of transitional Re of 62.4, 37.8, and 20.5 for the 10 PPI, 20 PPI, and 40 PPI foams, respectively. Using the third and final method of relating the Re to the average pore diameter gave the widest range of transitional Re of 725, 412, and 177 for the 10 PPI, 20 PPI, and 40 PPI metal foams, respectively.

Even though each method produces transitional Re within its respective order of magnitude, the best approach from these data is first method, which uses the permeability calculated at the transitional flow velocity. This method provides the narrowest transitional Re number range ($\sim$O(10)) with an easily calculable scheme. The only drawback is that one must perform experiments just beyond the transition point in order to witness the deviation of the $(\Delta P/Lv)$ plot.

Permeability and Form Coefficient Flowrate Dependence. Previous works which investigated the hydraulic characteristics of highly porous media found that values for the permeability and form coefficient of the porous medium depend upon the flow velocity range over which they are calculated [27]. The permeability and form coefficient were calculated for each compressed and uncompressed foam by varying the flow velocity range over which the terms were calculated to investigate this dependence. For the compressed foam samples, each calculation used the range of flow velocities from the common minimum, 0.010 m/s, to varying maxima at which the data points are plotted. Figures 9 and 10 plot the permeability and form coefficient against the fluid flow velocity for the compressed foams, beginning at 0.010 m/s and continuing to 1.042 m/s.

Looking at the permeabilities plotted against the fluid flow velocity for the compressed foam blocks in Fig. 9, it becomes immediately apparent that the range over which the permeability is calculated affects its value. The relatively flat region of the permeability located near the low end of the range marks the linear pressure-drop flow regime where Darcy's law holds. The value of the permeability reaches a maximum at a value of the Darcian flow velocity of approximately 0.2 m/s. For example, at this flow velocity, foam 95-02 has a peak permeability of $175\times10^{-10}\,\mathrm{m}^2$. After this peak, all permeabilities decrease and level off to their respective values which are tabulated in Table 2 and were obtained using the entire flowrate range tested (up to 1.042 m/s fluid flow velocity). A possible explanation for this peak and the fol-

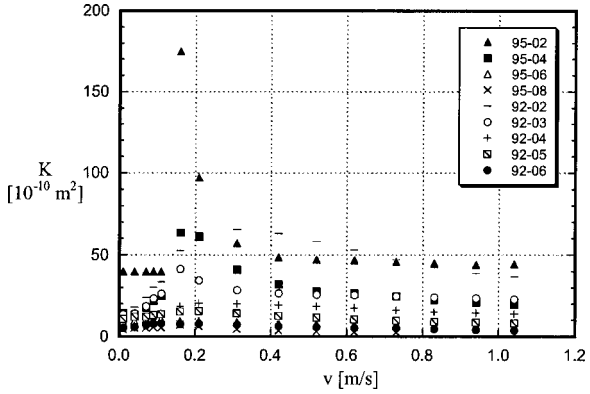

Fig. 9 Plot of the permeability, *K*, for the compressed aluminum foam blocks using a maximum flow velocity which corresponds to the velocity value at which the *K* value is plotted

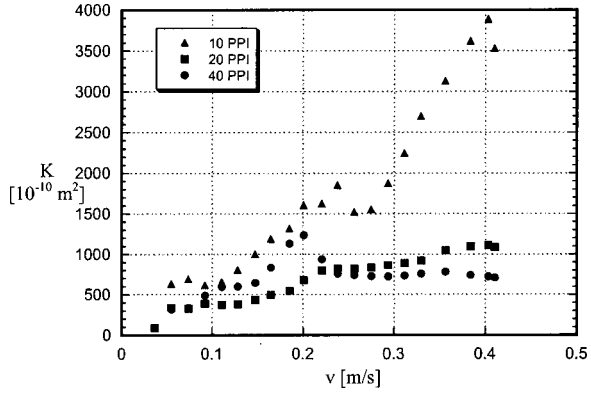

Fig. 11 Plot of the permeability, *K*, for the uncompressed aluminum foam blocks using a maximum flow velocity which corresponds to the velocity value at which the *K* value is plotted

lowing decrease in value may be offered by the least-squares method of calculating the permeability-based Reynolds number, Re_K. Forcing a curve fit onto data points which are comparably weighted in both the linear and quadratic regimes caused this peak to arise in the region of the transition points. When more points are accumulated in the quadratic region, i.e., as the fluid flow velocity continues to increase after the transition point, the majority of the curve-fitting points in the quadratic region then dominate and the permeability converges to its ultimate value.

The behavior of the form coefficients of the compressed foam samples in Fig. 10 mimicked the behavior of the changes in permeability in Fig. 9, which showed a trend of rising values until peaking at a fluid flow velocity of approximately 0.2 m/s. After this peak, the form coefficients of all foam blocks converged in a monotonic fashion to their respective values which were obtained by using the entire flowrate range (up to 1.042 m/s). These form coefficient values obtained from the calculation over the entire flowrate range are given in Table 2. This behavior in the lower flow velocity range may be explained by the same reasoning for the initial rise in the permeability, i.e., the flow is passing through the transition point into the quadratic-dominated flow regime. Forcing a curve fit onto the data points which are comparably weighted in both the linear and quadratic regimes caused these peaks to develop around the transition points.

The same permeability and form coefficient calculation process was used for the data sets of the uncompressed foam blocks. However, the flowrates spanned from 1.000 l/min. to 11.220 l/min., which corresponded to Darcian flow velocities from 0.037 m/s to 0.410 m/s. The permeability, which is plotted at the lowest flow velocity (0.037 m/s), is based only on that single data point. The rest of the calculated permeabilities include all data points between the lowest flow velocity of 0.037 m/s and up to and including the flow velocity at which the respective permeability value is plotted. Figure 11 plots the permeability based on an increasing maximum fluid flow speed. The permeabilities of the three uncompressed foams are nearly constant in the lower fluid flow speed range, up to the flow speed of approximately 0.1 m/s, which was previously explained as being the range in which the fluid enters the quadratic pressure-drop regime. The values of the permeability for the 20 PPI and 40 PPI foams peak at a fluid flow velocity of approximately 0.2 m/s, and then decline and remain somewhat steady for the rest of the flow speed range tested, up to 0.410 m/s. This behavior resembles the behavior of the compressed metal foams, as seen in Fig. 9, and indicates that the quadratic curve fits well to the data. The permeability of the 10 PPI foam, however, continued to rise after the transitional fluid flow velocity of 0.101 m/s, ultimately peaking just short of the maximum fluid flow speed tested, 0.410 m/s.

Figure 12 plots the form coefficients for the three uncompressed foams. The values of the form coefficient of all three foams start at a value of nearly zero and then increase up to a fluid flow velocity of approximately 0.2 m/s. Here the form coefficients obtain a maximum value and remain constant for the rest of the fluid flow speed tested, up to 0.410 m/s. As previously explained, decreasing the pore diameter consistently increased the flow resistance, and this change was also reflected in the changing form

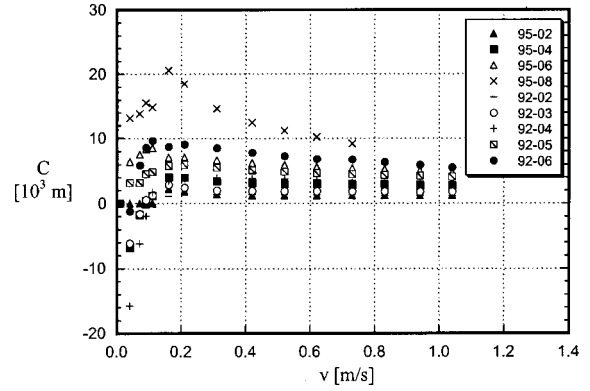

Fig. 10 Plot of the form coefficient, *C*, for the compressed aluminum foam blocks using a maximum flow velocity which corresponds to the velocity value at which the *C* value is plotted

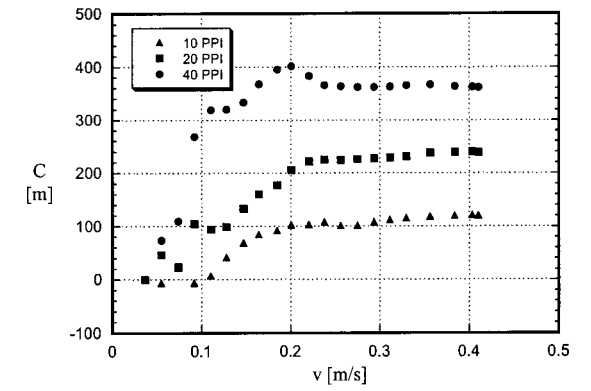

Fig. 12 Plot of the form coefficient, *C*, for the uncompressed aluminum foam blocks using a maximum flow velocity which corresponds to the velocity value at which the *C* value is plotted

coefficients. The 10 PPI foam, which had the largest pore diameter of 6.9 mm and the smallest specific surface area of 820 m^2/m^3, also had consistently the lowest form coefficient, with an ultimate value of 120 m^{-1}. The 40 PPI foam, which had the smallest pore diameter of 2.3 mm and the largest specific surface area of 2700 m^2/m^3, consistently generated the largest form coefficient, with an ultimate form coefficient value of 362 m^{-1}. This behavior was already witnessed in the discussion of Fig. 7, whereby increasing the surface area increased the total drag. The steadiness of the form coefficient beyond the fluid flow speed range of approximately 0.22 m/s indicates a good quadratic curve-fit to the data and validates the use of the quadratic pressure-drop relation, Eq. (5), as long as the flowrate range used in the calculation extends beyond the transition point.

Uncertainty Analysis

The uncertainties generated by the least-squares curve fit are given by the general formula for error propagation [29] applied to the least-squares curve fit equations, Eqs. (9) and (10), which yields the following equations for the uncertainty of the A and B coefficients of Eq. (8).

$$\Delta A = \sqrt{\sum_{i=1}^{n}\left(\frac{\partial A}{\partial x_i}\Delta x_i\right)^2 + \sum_{i=1}^{n}\left(\frac{\partial A}{\partial y_i}\Delta y_i\right)^2} \tag{15}$$

$$\Delta B = \sqrt{\sum_{i=1}^{n}\left(\frac{\partial B}{\partial x_i}\Delta x_i\right)^2 + \sum_{i=1}^{n}\left(\frac{\partial B}{\partial y_i}\Delta y_i\right)^2} \tag{16}$$

Each i term represents a single data pair (Darcy flow velocity and length-normalized pressure). The corresponding partial derivatives of Eqs. (9) and (10) were calculated and inserted into Eqs. (15) and (16) in order to obtain ΔA and ΔB. Backsolving A for K in Eq. (6) yields the uncertainty for the permeability. Assuming zero uncertainty for the dynamic viscosity, this gives the following relationship.

$$\sigma_K = \frac{\Delta A}{A} \times 100\% \tag{17}$$

The uncertainty of the form coefficient is given by backsolving Eq. (7) and applying the same error propagation technique as in Eqs. (15) and (16). Assuming zero uncertainty in the density term gives the uncertainty of the form coefficient as

$$\sigma_C = \frac{\Delta B}{B} \times 100\% \tag{18}$$

The uncertainties of the permeabilities and the form coefficients are tabulated in Table 2.

Conclusions

Open-cell metal foams were experimentally tested to evaluate their hydraulic characteristics using water. The experimental matrix of metal foams consisted of open-cell aluminum foams of various porosities and pore diameters in both compressed and uncompressed form. The characterization procedure involved solving for two terms, the permeability and the form coefficient. These two factors accurately described the pressure-drop vs. flow velocity behavior in porous media in general and were shown to be applicable to high porosity metal foams. From these experiments and the reduction of the data, several conclusions can be drawn.

1 The structural differences in the precompressed form between the originally 95% and 92% metal foams did not have a noticeable effect on the permeability. When comparing compressed foams with varying degrees of compression and initial porosities, the post-compression porosity governs the permeability and the resulting pressure-drop.

2 Similar compression factors had similarly weighted effects on both foams with 95% and 92% pre-compression porosity. Increasing the compression factor decreased the permeability of the foam by regular, incremental amounts, which were nearly equal for each of the two foam series.

3 The permeability of the compressed foams became more sensitive to changes in the porosity as the porosity increased.

4 Holding the porosity constant and decreasing the pore diameter increased the flow resistance in the uncompressed metal foams by reducing the permeability and increasing the form coefficient. This increase is attributed to the higher specific surface area generated by the smaller pore size.

5 The transition regime between the linear Darcy regime and the well-defined quadratic flow regime for all metal foams tested occurred in a Re_K range between unity and 26.5 based on the calculation of the permeability and form coefficient in this range.

6 The narrowest range of transitional Re_K was obtained when the permeability was calculated using a flowrate range from zero to the flow velocity at which the transition occurred.

7 Using different flow velocity regimes resulted in various permeability and form coefficient values. Whenever the permeability and the associated form coefficient for a high-porosity porous medium are stated, the flow velocity range over which these terms are calculated must also be specified for accuracy.

Acknowledgments

It is gratefully acknowledged that this research was supported jointly by the Swiss Commission for Technology and Innovation (CTI) through project no. 4150.2 and by the ABB Corporate Research Center, Baden-Dättwil, Switzerland. Helpful discussions with Dr. Fabian Zwick and Dr. Alexander Stuck of the ABB Corporate Research Center during the course of the work are also acknowledged.

Nomenclature

A = coefficient for curve fitting [$bar \cdot s \cdot m^{-2}$]
B = coefficient for curve fitting [$bar \cdot s \cdot m^{-3}$]
C = inertia coefficient [m^{-1}]
D = diameter [m]
K = permeability [m^2]
L = length [m]
M = compression factor
P = pressure [bar]
Q = volumetric flowrate [$m^3 s^{-1}$]
Re_K = permeability based Reynolds number [$\rho v K^{1/2} \mu^{-1}$]
Re_p = pore based Reynolds number [$\rho v D_p \mu^{-1}$]
v = velocity [ms^{-1}]

Greek

Δ = difference
ε = void fraction [range $1.0 \geqslant \varepsilon > 0.0$]
μ = dynamic viscosity [$kg \cdot m^{-1} s^{-1}$]
ρ = density [$kg \cdot m^{-3}$]
σ = uncertainty [%]

Subscripts

D = Darcy
K = permeability based
cs = cross-section
i = single, independent data point reference notation
p = pore diameter based

References

[1] Boomsma, K., and Poulikakos, D., 2001, "On the effective thermal conductivity of a three-dimensionally structured fluid-saturated metal foam," Int. J. Heat Mass Transf., **44**, pp. 827–836.
[2] Okuyama, M., and Abe, Y., 2000, "Measurement of Velocity and Temperature Distributions in a Highly Porous Medium," Journal of Porous Media, **3**, pp. 193–206.
[3] Schlegel, A., Benz, P., and Buser, S., 1993, "Wärmeübertragung und Druck-

abfall in keramischen Schaumstrukturen bei erzwungener Strömung,'' Wärme- und Stoffübertragung, **28**, pp. 259–266.
[4] Kaviany, M., 1995, *Principles of Heat Transfer in Porous Media*, Second ed., Springer-Verlag, New York.
[5] Lage, J. L., 1998, ''The Fundamental Theory of Flow Through Permeable Media from Darcy to Turbulence,'' *Transport Phenomena in Porous Media*, D. B. Ingham and I. Pop, eds., Elsevier Science, Oxford, pp. 1–30.
[6] Darcy, H., 1856, *Les Fontaines Publiques de la ville de Dijon*., Dalmont, Paris.
[7] Krüger, E., 1918, ''Die Grundwasserbewegung,'' Internationale Mitteilungen für Bodenkunde, **8**, pp. 105.
[8] Scheidegger, A. E., 1974, *The Physics of Flows Through Porous Media*, Third ed., University of Toronto Press, Toronto.
[9] Fand, R. M., Kim, B. Y. K., Lam, A. C. C., and Phan, R. T., 1987, ''Resistance to the Flow of Fluids through Simple and Complex Porous Media whose Matrices are Composed of Randomly Packed Spheres,'' ASME J. Fluids Eng., **109**, pp. 268–274.
[10] Macdonald, I. F., El-Sayed, M. S., Mow, K., and Dullien, F. A. L., 1979, ''Flow through porous media: The Ergun equation revisited,'' Ind. Eng. Chem. Fundam., **18**, pp. 199–208.
[11] Diedericks, G. P. J., and Du Plessis, J. P., 1997, ''Modeling of flow through homogeneous foams,'' Mathematical Engineering in Industry, **6**, pp. 133–154.
[12] Dupuit, J., 1863, *Etudes Theoriques et Pratiques sur le Mouvement des Eaux*., Dunod, Paris.
[13] Beckermann, C., and Viskanta, R., 1986, ''Forced convection boundary layer flow and heat transfer along a flat plate embedded in a porous medium,'' Int. J. Heat Mass Transf., **30**, pp. 1547–1551.
[14] Amiri, A., and Vafai, K., 1994, ''Analysis of dispersion effects and non-thermal equilibrium, non-Darcian, variable porosity incompressible flow through porous media,'' Int. J. Heat Mass Transf., **37**, pp. 939–954.
[15] Mehta, D., and Hawley, M. C., 1969, ''Wall effect in packed columns,'' I & EC Process Design and Development, **8**, pp. 280–282.
[16] Baumeister, J., 1997, ''Überblick: Verfahren zur Herstellung von Metallschäumen,'' presented at Symposium Metallschäume, J. Banhart, Verlag Metall Innovation Technologie, Bremen, pp. 3–14.
[17] Ergun, S., 1952, ''Fluid Flow through Packed Columns,'' Chem. Eng. Prog., **48**, pp. 89–94.
[18] Renken, K., and Poulikakos, D., 1988, ''Experiment and analysis of forced convective heat transport in a packed bed of spheres,'' Int. J. Heat Mass Transf., **31**, pp. 1399–1408.
[19] Poulikakos, D., and Renken, K., 1987, ''Forced Convection in a Channel Filled With Porous Medium, Including the Effects of Flow Inertia, Variable Porosity, and Brinkmann Friction,'' ASME J. Heat Transfer, **109**, pp. 880–888.
[20] Du Plessis, J. P., Montillet, A., Comiti, J., and Legrand, J., 1994, ''Pressure Drop Prediction for Flow through High Porosity Metallic Foams,'' Chem. Eng. Sci., **49**, pp. 3545–3553.
[21] Smit, G. J. F., and du Plessis, J. P., 1999, ''Modeling of non-Newtonian purely viscous flow through isotropic high porosity synthetic foams,'' Chem. Eng. Sci., **54**, pp. 645–654.
[22] Sodre, J. R., and Parise, J. A. R., 1997, ''Friction factor determination for flow through finite wire-mesh woven-screen matrices,'' ASME J. Fluids Eng., **119**, pp. 847–851.
[23] Dybbs, A., and Edwards, R. V., 1975, ''Department of Fluid, Thermal, and Aerospace Report,'' presented at Workshop on Heat and Mass Transfer in Porous Media, FTAS/TR (Case Western Reserve University), Springfield, VA., pp. 75–117.
[24] Lage, J. L., Antohe, B. V., and Nield, D. A., 1997, ''Two Types of Nonlinear Pressure-Drop Versus Flow-Rate Relation Observed for Saturated Porous Media,'' ASME J. Fluids Eng., **119**, pp. 700–706.
[25] Forchheimer, P., 1901, ''Wasserbewegung durch Boden,'' Z. Ver. Deutsch. Ing., **45**, pp. 1736–41 pp. 1781–1788.
[26] Givler, R. C., and Altobelli, S. A., 1994, ''A determination of the effective viscosity for the Brinkmann-Forchheimer flow model,'' J. Fluid Mech., **258**, pp. 355–370.
[27] Antohe, B. V., Lage, J. L., Price, D. C., and Weber, R. M., 1997, ''Experimental Determination of Permeability and Inertia Coefficients of Mechanically Compressed Aluminum Porous Matrices,'' ASME J. Fluids Eng., **119**, pp. 404–412.
[28] 1999, *Duocel Aluminum Foam Data Sheet*., ERG Material and Aerospace, Oakland.
[29] Taylor, J. R., 1997, *An Introduction to Error Analysis*, Second ed., University Science Books, Sausalito.